Reviews in Mineralogy & Geochemistry
Vol. 71 pp. 253-269, 2010

Theoretical Methods for Calculating the Lattice Thermal Conductivity of Minerals

Stephen Stackhouse

Department of Earth and Planetary Science
University of California, Berkeley
307 McCone Hall
Berkeley, California, 94720-4767, U.S.A.

s.stackhouse@berkeley.edu

Lars Stixrude

Department of Earth Sciences
University College London
Gower Street, London, WC1E 6BT, United Kingdom

ABSTRACT

The thermal conductivity of the lower mantle plays a major role in shaping the structure and dynamics of the region. However, the thermal conductivity of lower mantle minerals are, at present, not well constrained, because of difficulties in making measurements at such high pressures. Here we describe the most common theoretical methods available to calculate the thermal conductivity of materials, which provide an invaluable alternative to experimental techniques. In each case the general scheme is given and particular considerations highlighted. The advantages and disadvantages and applicability of the methods are then discussed. We conclude with a short review of theoretical studies of the lattice thermal conductivity of periclase.

INTRODUCTION

The bulk of the lower mantle is composed of ferropericlase and ferromagnesian silicate perovskite (Lee et al. 2004). To understand the lower mantle it is, therefore, essential to constrain the properties of these phases. Of particular importance are their thermal transport properties, which have, from formation, played a major role in shaping the deep Earth. Following segregation, the thermal conductivity of the lower mantle regulated the heat flux from the core and thus had a significant influence on thermal evolution, in particular on the rate of growth of the solid inner core (Lay et al. 2008). In the present Earth, thermal conductivity plays a significant role in determining the structure and dynamics of the lower mantle, controlling the size and stability of thermal upwellings (Dubuffet et al. 1999; Dubuffett and Yuen 2000; Naliboff and Kellogg 2006, 2007). In addition, lateral variations in the thermal structure of the lowermost mantle, which could be related to lateral variations in thermal conductivity, have been shown to influence magnetic field generation (Gubbins et al. 2007; Willis et al. 2007).

The thermal conductivity of the lower mantle can be decomposed into two principle components. The first is the lattice contribution, related to thermal conduction by phonons (lattice vibrations). The second is the radiative contribution related to thermal conduction by photons (electromagnetic radiation). Conduction of heat by electrons is expected to be negligible. The lattice thermal conductivity of ferropericlase and ferromagnesian silicate perovskite has not been measured at lower mantle temperatures and pressures, and geophysical

1529-6466/10/0071-0012$05.00 DOI: 10.2138/rmg.2010.71.12

values are estimated by model extrapolations from low-pressure data (Hofmeister 2007, 2008; Goncharov et al. 2009). Experimental measurements of radiative thermal conductivity remain inconclusive. Though there is general agreement that the high-to-low-spin transition in iron decreases radiative conductivity (Goncharov et al. 2006; Keppler et al. 2007), instead of increasing it as was first thought (Badro et al. 2003, 2004), disagreement remains on values in the low-spin regime. Measurements of the radiative conductivity of silicate perovskite differ by an order of magnitude (Goncharov et al. 2008; Keppler et al. 2008). However, even if the higher values are adopted, it seems probable that the lattice contribution dominates at lower mantle conditions.

Numerous theoretical techniques for determining lattice thermal conductivity have been reported in the literature (e.g., Evans and Morris 1990; Müller-plathe 1997; Daly et al. 2002; Nieto-Draghi and Avalos 2003; de Koker 2009; Tang and Dong 2009) and have been applied to a wide range of materials. However, their application to lower mantle phases is a relatively recent development with only a handful of studies published (Cohen 1998; Shukla et al. 2008; Stackhouse et al. 2008; de Koker 2009; Tang and Dong 2009), all of which focus on periclase, the pure magnesium end-member of ferropericlase. The purpose of the present work is to provide an overview of the most popular theoretical methods for calculating lattice thermal conductivity, discussing their underlying theories, relative merits and shortcomings and highlighting possible pitfalls. In addition, the few theoretical studies of periclase are reviewed. The overall aim is to equip the reader with the knowledge required to select and use the most appropriate method in their own work, after considering the computational resources and time available to them.

FUNDAMENTAL PRINCIPLES

Imagine that a temperature gradient is imposed across a solid, heat flows from the hotter region to the cooler one. Fourier's Law states that the magnitude of the induced heat flux will be proportional to the temperature gradient, and defines thermal conductivity as the property of the solid that relates the two

$$q_i = -k_{ij} \frac{\partial T}{\partial x_j} \tag{1}$$

where q_i is the heat flux, $\partial T/\partial x_j$ the temperature gradient and k_{ij} the second-rank thermal conductivity tensor. For those materials of cubic or isotropic symmetry the thermal conductivity tensor is isotropic (Nye 1957), such that

$$k_{ij} = k\delta_{ij} \tag{2}$$

and thus Fourier's law reduces to

$$q = -k \frac{\partial T}{\partial x} \tag{3}$$

where the temperature gradient and heat flux are in the same direction.

It should be noted that Fourier's law is only applicable to systems in steady-state. For systems out of steady-state we must use the heat conduction equation (Holman 1976; Kreith and Bohn 2001). Focusing on the conductive contribution to heat transfer, for an isotropic system, the heat conduction equation reads

$$\frac{\partial}{\partial x_i}\left(k \frac{\partial T}{\partial x_j} \right)\delta_{ij} = \rho c_P \frac{\partial T}{\partial t} \tag{4}$$

where ρ is the density and C_P the isobaric specific heat. For small homogeneous crystals the spatial gradient in k may be neglected. Taking this into account, and dividing both sides by ρC_P leads to

$$\frac{\partial T}{\partial t} = D\frac{\partial^2 T}{\partial x^2} \tag{5}$$

where D is the thermal diffusivity, related to k via

$$D = \frac{k}{\rho C_P} \tag{6}$$

The phonon contribution to thermal conductivity is related to microscopic dynamics via (Ziman 1960; Srivastava 1990)

$$k = \sum_{\mathbf{q}} \sum_{s=1}^{3N} c_{\mathbf{q},s} v_{\mathbf{q},s}^2 \tau_{\mathbf{q},s} \tag{7}$$

where the sum is over all wave vectors $\mathbf{q}$ and $3N$ polarization indices s (N is the number of atoms in the primitive cell); $v_{\mathbf{q},s}$ the group velocity and $\tau_{\mathbf{q},s}$ the relaxation time associated with each mode. The mode contribution to the heat capacity is

$$c_{\mathbf{q},s} = \frac{k_B}{V}\frac{x^2 e^x}{(e^x - 1)^2}; \quad x = \frac{h\omega_{\mathbf{q},s}}{k_B T} \tag{8}$$

where $\omega_{\mathbf{q},s}$ is the frequency of the mode; k_B Boltzmann's constant; h Planck's constant; V volume; and T temperature. At lower mantle temperatures, and for typical lower mantle minerals, the mode heat capacities all take on the high temperature limiting value and lattice thermal conductivity may be written as

$$k = \frac{1}{3} C_v \left\langle v^2 \tau \right\rangle \tag{9}$$

where C_v is the bulk volumetric isochoric heat capacity and the brackets indicate the average over all modes, or as

$$k = \frac{1}{3} C_v \left\langle v \Lambda \right\rangle \tag{10}$$

where $\Lambda = v\tau$ is the phonon mean free path.

THEORETICAL METHODS

In this section we describe the most widely used theoretical methods for calculating lattice thermal conductivity. These are based on either molecular dynamics or lattice dynamics or both, and it is assumed that the reader has a working knowledge of these and concepts associated with them. Information on these topics can be found elsewhere (e.g., Allen and Tildesley 1987; Leach 2001). The descriptions given below are not exhaustive and additional details can be found in some excellent reviews (McGaughey and Kaviany 2006; Chantrenne 2007).

Green-Kubo method

In an equilibrium molecular dynamics simulation the system under investigation has a constant average temperature and an average heat flux of zero. However, at each instant of time a finite heat flux exists due to instantaneous fluctuations in temperature. The popular Green-Kubo method (Green 1954; Kubo 1957), based on the general fluctuation-dissipation theorem

(Kubo 1966), relates the lattice thermal conductivity of the system to the time required for such fluctuations to dissipate

$$k_{ij} = \frac{V}{k_B T^2} \int_0^\infty \left\langle q_i(0) q_j(t) \right\rangle dt \tag{11}$$

where k_{ij} is a component of the lattice thermal conductivity tensor (i and $j = x$, y or z), V the volume of the system, k_B Boltzmann's constant, T the temperature of the system, $q_i(0)$ the instantaneous heat flux in the j direction at time zero and $q_j(t)$ the instantaneous heat flux in the i direction at time t. The angular brackets on the right-hand-side indicate an average over time origins. Though the upper limit on the integral is infinite the duration of the simulation must only exceed the relaxation time beyond which the integrand vanishes (Fig. 1). In molecular dynamics simulations time is discretized into time-steps, and thus in practice Equation (11) becomes a summation (Schelling et al. 2002)

$$k_{ij} = \frac{V \Delta t}{k_B T^2} \sum_{m=1}^{M} (N-m) \sum_{n=1}^{N-m} q_i(m+n) q_j(n) \tag{12}$$

where N is the total number of time-steps, each of length Δt, $q_i(m+n)$ the instantaneous heat flux in the i direction at time-step $m+n$ and $q_j(n)$ the instantaneous heat flux in the j direction at time-step n. The instantaneous heat flux, in a given direction, is evaluated from the energy associated with each atom in the simulation

$$\mathbf{q} = \frac{d}{dt} \frac{1}{V} \sum_{i=1}^{N} \mathbf{r}_i \varepsilon_i \tag{13}$$

where $\mathbf{q}$ is the heat flux vector, $\mathbf{r}_i$ the position vector of atom i and ε_i the energy associated with atom i, and the sum is over all N atoms. The energy associated with each atom is the sum of its

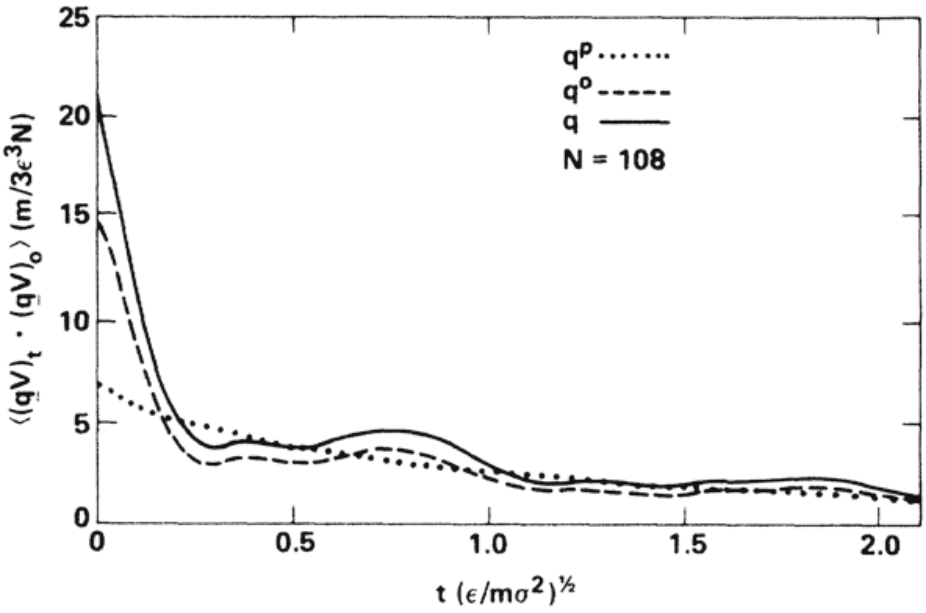

Figure 1. Heat flux autocorrelation function (solid line) of a Lennard-Jones fcc crystal at $T = 0.546\varepsilon/k_B$ or about 25 percent of the melting point, density $N/V = (2)^{1/2}/\sigma^3$, and $N = 108$. Time is non-dimensionalized such that one vibrational period of about $0.25(m\sigma^2/\varepsilon)^{1/2}$. The two dashed lines represent approximations to the auto-correlation function that are valid in the limit of low temperature. m is the atomic mass, σ is the Lennard-Jones length scale and ε is the Lennard-Jones energy scale. Reprinted with permission from Ladd et al. (1986) Physical Review B, Vol. 34, p 5058-5064. Copyright 1986 by the American Physical Society. *http://link.aps.org/doi/10.1103/PhysRevB.34.5058*

kinetic energy and potential energy

$$\varepsilon_i = \frac{1}{2} m_i \mathbf{v}_i^2 + \frac{1}{2} \sum_j^N u_{ij}(r_{ij}) \tag{14}$$

where m_i is the mass of atom i, $\mathbf{v}_i$ the velocity vector of atom i, and $u_{ij}(r_{ij})$ the pair-wise interaction between atoms i and j when separated by a distance r_{ij}. Substituting Equation (14) into Equation (13) we obtain

$$\mathbf{q} = \frac{1}{V}\left[\sum_i^N \mathbf{v}_i \varepsilon_i + \frac{1}{2} \sum_i^N \sum_{j \neq i}^N \mathbf{r}_{ij} (\mathbf{F}_{ij} \bullet \mathbf{v}_i) \right] \tag{15}$$

where $\mathbf{r}_{ij} = \mathbf{r}_i - \mathbf{r}_j$ and $\mathbf{F}_{ij}$ is the force exerted on atom i by atom j. The first term within the square brackets is related to convection and the second to conduction. For more complex potentials additional terms are required (Schelling et al. 2002).

It important to note that in Green-Kubo calculations, just as in many simulation studies, finite-size effect are important and that calculated values converge towards experimental values with increasing system size (Volz and Chen 2000; Sun and Murthy 2006). Such convergence must be checked for in order ensure that calculated values are accurate.

Non-equilibrium molecular dynamics

Non-equilibrium molecular dynamics is the most intuitive theoretical method for determining lattice thermal conductivity, in that it calculates it from the ratio of a heat flux to a temperature gradient, similar to what is done in experimental studies. The simulations can take one of two approaches: either a known heat flux is imposed and the resulting temperature gradient is calculated or a fixed temperature gradient is imposed and the heat flux required to maintain it calculated. However, the former is more usual and we focus on it here.

In general, molecular dynamics simulations are performed in conjunction with a periodic simulation cell, representing the structure of the system under investigation. In such a context, the most common approach to imposing a heat flux is to divide the simulation cell into an even number of equal-size sections, designate one as the hot section and another, half a simulation cell length along, as the cold section, and at regular intervals in time transfer heat from the cold section to the hot section (Fig. 2:A). Since the simulation cell is periodic, heat leaves both sides of the hot section and enters both sides of the cold section, leading to the generation of two heat fluxes in opposing directions and two corresponding temperature gradients (Fig. 2:B).

There are a number of different schemes for transferring heat from the hot section to the cold section. One of the most popular methods involves the regular transfer of heat from the hottest atom in the cold section to the coldest atom in the hot section (Müller-plathe 1997; Nieto-Draghi and Avalos 2003). In particular, at intervals of a fixed number of time-steps, the hottest atom in the cold section is imagined to undergo an elastic collision with the coldest atom in the hot section and the velocities arising from such a collision assigned to the atoms prior to continuation of the simulation. The post-collision velocity of the atom in the cold section is calculated as

$$\mathbf{v}_c' = -\mathbf{v}_c + 2\left[\frac{m_c \mathbf{v}_c + m_h \mathbf{v}_h}{m_c + m_h} \right] \tag{16}$$

and that of the atom in the hot section as

$$\mathbf{v}_h' = -\mathbf{v}_h + 2\left[\frac{m_c \mathbf{v}_c + m_h \mathbf{v}_h}{m_c + m_h} \right] \tag{17}$$

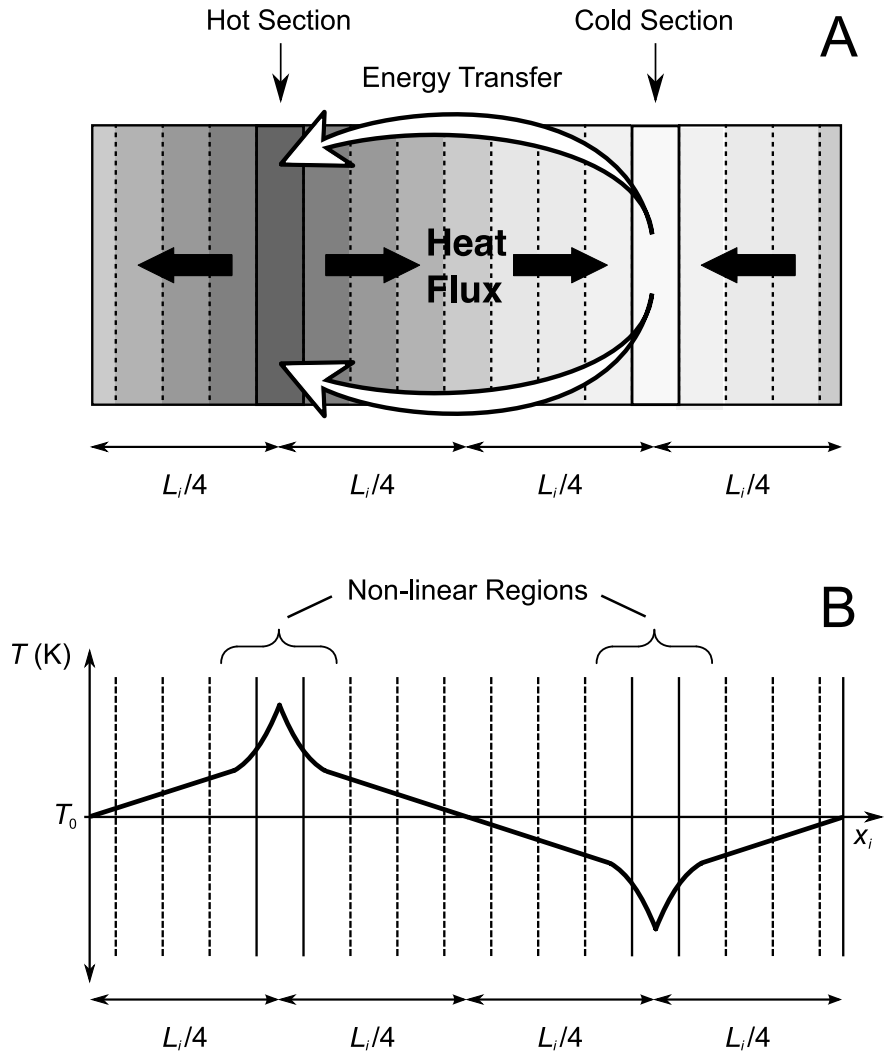

Figure 2. Typical set-up in a non-equilibrium molecular dynamic simulation (A) and resulting temperature profile (B). The simulation cell is divided into sections of equal dimensions, one is designated the 'hot section', another the 'cold section' and at regular intervals heat is transferred from the cold section to the hot section, by modification of the velocities of some or all of the atoms in the two sections. The temperature gradient is non-linear around the hot and cold sections due to the non-Newtonian nature of the heat transfer. Only the linear portion of the temperature gradient is used in the calculation of thermal conductivity.

where m_c and m_h are the respective masses of the atoms in the cold and hot sections, $\mathbf{v}_c$ and $\mathbf{v}_h$ their velocities before the collision and $\mathbf{v}_c'$ and $\mathbf{v}_h'$ their velocities after it. The reasons for using such a construct is that Equations (16) and (17) enable the exchange of heat between the sections, while conserving the total kinetic energy, potential energy and linear momentum of the system. The average heat flux is then determined from

$$q_i = \frac{1}{2AN\Delta t} \sum_{n=1}^{N/\nu_t} \frac{1}{2} m_h (\mathbf{v}_h'(n\nu_t)^2 - \mathbf{v}_h(n\nu_t)^2) \tag{18}$$

where q_i is the average heat flux flowing in the i direction (where $i = x$, y or z), A the cross-sectional area of the simulation cell perpendicular to i, N the total number of time-steps, Δt the time-step, ν_t the frequency of the heat transfers in time-steps, and $\mathbf{v}_h(n\nu_t)$ and $\mathbf{v}_h'(n\nu_t)$ the velocities of the atom in the hot section before and after transfer at time-step $n\nu_t$. The factor half arises because heat flows from both sides of the hot section to both sides of the cold

section, with an average of half of the exchanged heat flowing in each of the two directions. Using this method it is impossible to know the resulting heat flux *a priori*. However, by varying the frequency of heat transfers, it is possible to control the magnitude of the heat-flux, and corresponding temperature gradient.

More control on the magnitude of the imposed heat flux is afforded in an alternative approach, which transfers heat from the cold section to the hot section by scaling the velocities of all of the atoms in the two sections (Jund and Jullien 1999). In particular, at regular intervals the velocities of the atoms in the hot and cold sections are adjusted according to

$$\mathbf{v}_i' = \mathbf{v}_G + \chi(\mathbf{v}_i - \mathbf{v}_G) \tag{19}$$

where $\mathbf{v}_i$ and $\mathbf{v}_i'$ are the velocities of atom i before and after rescaling; $\mathbf{v}_G$ is the velocity of the center of mass of the section before rescaling, computed from

$$\mathbf{v}_G = \frac{\sum_{i=1}^{N} m_i \mathbf{v}_i}{\sum_{i=1}^{N} m_i} \tag{20}$$

where the sum is over all N atoms in the hot or cold section, m_i is the mass of atom i, and χ a scaling coefficient given by

$$\chi = \sqrt{1 \pm \frac{\Delta\varepsilon}{\varepsilon_R}} \tag{21}$$

where $\Delta\varepsilon$ is the amount of heat to be transferred from the cold section to the hot section, and ε_R is the relative energy of the section, defined as

$$\varepsilon_R = \frac{1}{2}\sum_{i=1}^{N} m_i \mathbf{v}_i^2 - \frac{1}{2}\sum_{i=1}^{N} m_i \mathbf{v}_G^2 \tag{22}$$

In Equation (21) the sign is positive for the hot section and negative for the cold section. The heat flux is calculated from

$$q_i = \frac{\Delta\varepsilon}{2A\Delta t} \tag{23}$$

where A is the cross-sectional area of the simulation cell perpendicular to i, and Δt the time-step. The magnitude of $\Delta\varepsilon$ is chosen to give the desired temperature gradient.

For both of the above heat transfer methods, once steady-state is reached, lattice thermal conductivity is calculated from Fourier's Law in one dimension

$$q_i = -k_{ii} \frac{dT}{dx_i} \tag{24}$$

where the temperature gradient, dT/dx_i, is determined from the average instantaneous temperature of each section, T_S, calculated at each time-step from

$$T_S = \frac{1}{3k_B N}\sum_{i=1}^{N} m_i \mathbf{v}_i^2 \tag{25}$$

where the sum is over all N atoms located in the section.

The periodic nature of the simulation cell leads to two temperature gradients, equal in magnitude, but opposite in sign. It is normal to average the temperature of symmetrically equivalent sections to improve statistics. In some studies the difference in the average temperature

of symmetrically equivalent sections has been used as an indicator of whether or not steady state has been reached (e.g., Yoon et al. 2004). The process of energy transfer renders the dynamics in the immediate vicinity of the hot and cold sections non-Newtonian and the temperature profile in these regions non-linear (Fig. 2:B). In view of this, the temperature of the sections around the hot and cold sections are discarded during calculation of the temperature gradient. One practical consequence of this phenomenon is that, the simulation cell must be of a sufficient size for the temperature profile to have a linear portion.

The limited simulation cell size tractable with molecular dynamics methods often leads to the issue of finite-size effects. In particular, in calculations of lattice thermal conductivity, unless the length of the simulation cell is many times larger than the phonon mean-free path, one computes a value lower than the true value. This is because of the direct relationship between lattice thermal conductivity and phonon mean free path (Eqn. 10). In a real solid, the mean free path is mainly limited by phonon-phonon scattering, although phonon-defect scattering will also play a role when defects are present, but in non-equilibrium molecular dynamics simulations phonons are also scattered in the hot and cold sections. This leads to a lower mean free path, and thus lower lattice thermal conductivity. It is, however, possible to overcome this problem by performing simulations for cells of different sizes, as has also been done in a number of recent simulation studies (e.g., Schelling et al. 2002; Stackhouse et al. 2008).

The effective phonon mean free Λ_{eff} path for each simulation cell is expressed in terms of that related to phonon-phonon scattering $\Lambda_{ph\text{-}ph}$ and that related to phonon-boundary scattering $\Lambda_{ph\text{-}b}$, which occurs in the hot and cold sections

$$\frac{1}{\Lambda_{eff}} = \frac{1}{\Lambda_{ph-ph}} + \frac{1}{\Lambda_{ph-b}} \tag{26}$$

Since phonons can originate from any point between the hot and cold section and be scattered in the hot or cold sections, the distance that a phonon will travel between scattering events (in the absence of phonon-phonon interactions) will be, on average, one quarter of the length of the simulation cell in the direction of the heat-flux

$$\frac{1}{\Lambda_{eff}} = \frac{1}{\Lambda_{ph-ph}} + \frac{4}{L_i} \tag{27}$$

where L_i is the length of the simulation cell in the i direction. If we substitute Equation (27) into Equation (10) and rearrange, for an isotropic solid, we have

$$\frac{1}{k} = \left[\frac{12}{C_v v}\right]\frac{1}{L_i} + \left[\frac{1}{3}c_v v \Lambda_{ph-ph}\right]^{-1} \tag{28}$$

which means that a plot of k^{-1} against L_i^{-1} should be linear. Therefore by computing k for a range of L_i values, and plotting k^{-1} against L_i^{-1} it is possible to extrapolate to $L_i^{-1} = 0$ to determine the lattice thermal conductivity of a simulation cell of infinite size (Fig. 3), which should be comparable to the infinite-system value.

From a practical point of view, there are several important considerations that must made before performing non-equilibrium molecular dynamics simulations, necessitating some initial experimentation (Müller-Plathe 1997; Schelling et al. 2002; Chantrenne and Barrat 2004; Mountain 2006; Mahajan et al. 2007). The first is that one must choose the number of sections in which to divide the simulation cell. This is not straightforward. Larger sections will contain more atoms, leading to a more accurate estimate of their instantaneous temperature. On the other hand, larger sections will mean fewer sections in total, and thus less data points

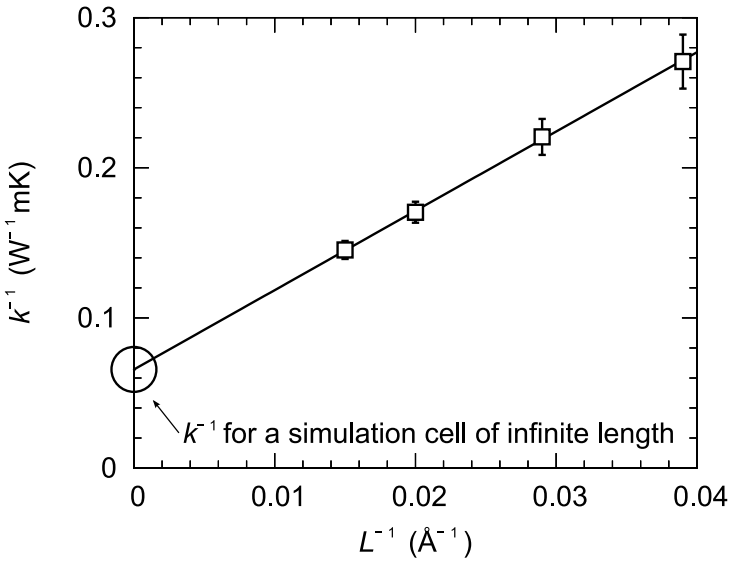

Figure 3. Typical plot of k^{-1} against L^{-1} obtained from a series non-equilibrium molecular dynamics simulation, using simulation cells of different size. Extrapolating back to $L^{-1} = 0$ it is possible to estimate the lattice thermal conductivity of a simulation cell of infinite size, accounting for the artificial phonon-boundary scattering introduced by the heat transfer mechanism.

from which to calculate the temperature gradient. The magnitude of the heat flux is also a concern. Imposing a large heat flux will lead to a large temperature gradient and much faster convergence. However, Fourier's Law is invalid for perturbations outside the linear response regime and care must be taken to ensure that it is still applicable. To assess this one can perform a series of simulations using heat fluxes of decreasing magnitude and check that the calculated lattice thermal conductivity is the same in each case. It is also worth noting that if the temperature gradient is large, then it will be unclear to which temperature the calculated lattice thermal conductivity corresponds. The effect of the size of the cross-sectional area perpendicular to the heat-flux is another factor that is also sometimes considered. This and each of the above factors must be investigated for each system and chosen with care.

Transient non-equilibrium molecular dynamics

In a similar manner to the non-equilibrium molecular dynamics method, the transient non-equilibrium molecular dynamics method (Daly and Maris 2002; Daly et al. 2002) begins by dividing a simulation cell into sections. However, instead of introducing a hot and cold section and imposing a constant one-dimensional heat flux, a sinusoidal temperature perturbation is applied across the sections and lattice thermal conductivity is determined from the rate at which the system re-equilibrates (Fig. 4).

The sinusoidal temperature perturbation is applied to the system according to

$$T(x_i) = T_0 + \Delta T_0 \cos\left[\frac{2\pi x_i}{L_i}\right] \tag{29}$$

where $T(x_i)$ is the temperature a distance x_i across the simulation cell, in the i direction (where $i = x$, y or z), T_0 the equilibrium temperature, ΔT_0 the amplitude of the sinusoidal temperature perturbation and L_i the length of the simulation cell in the i direction. Once applied, the system is allowed to re-equilibrate and the decrease in the amplitude of the sinusoidal temperature perturbation computed as a function of time from

$$\Delta T(t) = \frac{2}{L_i}\int_0^{L_i} T(x_i,t)\cos\left[\frac{2\pi x_i}{L_i}\right] dx_i \tag{30}$$

where $T(x_i,t)$ is the temperature a distance x_i across the simulation cell in the i direction, at a time t.

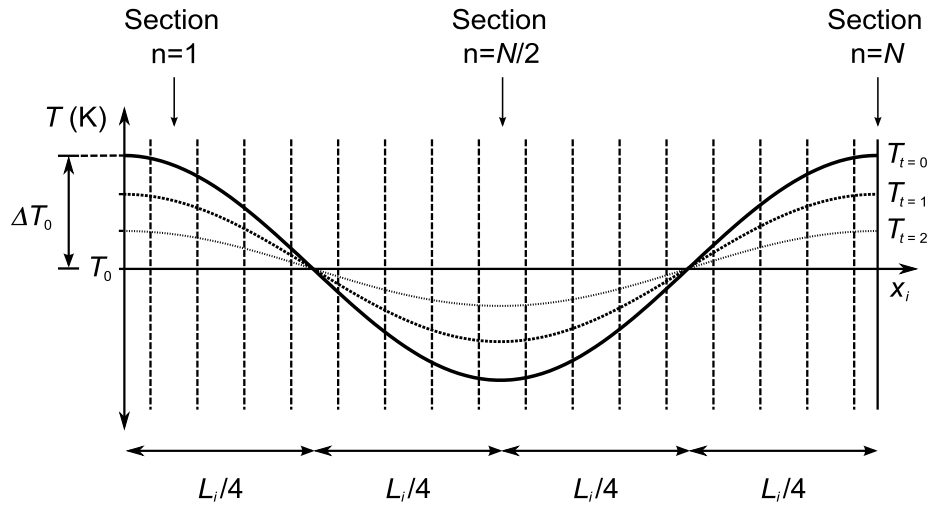

Figure 4. Typical procedure in a transient non-equilibrium molecular dynamics simulation. The system is brought to equilibrium at a temperature of T_0. Then a sinusoidal temperature perturbation of amplitude ΔT_0 is applied, across the simulation cell, and thermal conductivity determined from that rate at which the system re-equilibrates.

The rate at which such a system re-equilibrates can be related to its thermal diffusivity by solving the appropriate heat conduction equation (Holman 1976; Kreith and Bohn 2001)

$$\frac{\Delta T(t)}{\Delta T_0} = e^{-D_{ii}\left(\frac{2\pi}{L_i}\right)^2 t} \tag{31}$$

where D_{ii} is a component of thermal diffusivity tensor. Taking the logarithm gives

$$\ln\left[\frac{\Delta T(t)}{\Delta T_0}\right] = -D_{ii}\left(\frac{2\pi}{L_i}\right)^2 t \tag{32}$$

which allows the determination of D_{ii} from a simple plot of $\ln(\Delta T(t)/\Delta T_0)$ against t. The lattice thermal conductivity of the system can then be calculated from Equation (6), provided that its specific heat capacity and density are known.

In practice, the simulation cell is divided into N sections in the i direction, each of width L_i/N, which we label 1 to N and time is discretized into time-steps, each of length Δt. In this context the initial temperature profile is expressed as

$$T(n) = T_0 + \Delta T_0 \cos\left[\frac{2\pi n}{N}\right] \tag{33}$$

where $T(n)$ is the temperature of section n. The temperature perturbation is applied by rescaling the velocities of all atoms in each section, according to

$$\frac{\mathbf{v}_n'}{\mathbf{v}_n} = \sqrt{\frac{T(n)}{T_0}} \tag{34}$$

where $\mathbf{v}_n$ and $\mathbf{v}_n'$ are the velocities of atoms in section n before and after rescaling. The amplitude of the sinusoidal temperature perturbation is computed as

$$\Delta T(m) = \frac{2}{L_i}\sum_{n=1}^{N} T(n,m)\cos\left[\frac{2\pi n}{N}\right] \tag{35}$$

where $\Delta T(m)$ is the amplitude of the sinusoidal temperature perturbation at time-step m and $\Delta T(n,m)$ the instantaneous temperature of section n at time-step m computed from Equation (25). Thermal diffusivity is then determined from

$$\frac{\Delta T(m)}{\Delta T_0} = e^{-D_{ii}\left(\frac{2\pi}{L_i}\right)^2 m\Delta t} \tag{36}$$

where the time t is replaced by the product of the time-step number m and length Δt.

In addition to similar issues to those encountered in non-equilibrium molecular dynamics simulations, the transient molecular dynamics method suffers from a number of other complications. The sinusoidal temperature perturbation imposes a corresponding sinusoidal variation in thermal pressure across the simulation cell, which upon re-equilibration induces a low frequency vibrational mode, causing atoms to vibrate in the i direction (Daly and Maris 2002; Daly et al. 2002). However, the effect is expected to be small, and can be reduced by using smaller perturbations. More worrisome is an issue regarding the fitting of Equation (36) at short and long times scales, which can only been remedied by applying an *ad hoc* modification to the equation (Daly and Maris 2002; Daly et al. 2002).

Combined Quasiharmonic Lattice Dynamics and Molecular Dynamics Method

In lattice dynamics calculations the potential energy of a system is expressed as a Taylor series expansion of atomic displacements (Maradudin et al. 1963)

$$V = V^0 + \sum_{l,\kappa,i} \frac{\partial V}{\partial u_{l,\kappa,i}} + \frac{1}{2} \sum_{l,\kappa,i;l',\kappa',j} \frac{\partial^2 V}{\partial u_{l,\kappa,i} \partial u_{l',\kappa',j}} u_{l,\kappa,i} u_{l',\kappa',j} + \ldots \tag{37}$$

where V is the potential energy of the system; V^0 the potential energy of the system with all the atoms in their equilibrium positions, $u_{l,\kappa,i}$ the displacement of atom κ in unit cell l in the i direction (where $i = x$, y or z) and $u_{l',\kappa',j}$ the displacement of atom κ' in unit cell l' in the j direction (where $j = x$, y or z). Since the derivatives are evaluated with the atoms at their equilibrium positions, by definition, the first derivative must be zero. It is usual to truncate the expansion at the second derivative as is shown, making what is known as the quasiharmonic approximation.

The second term on the right hand side represents the harmonic inter-atomic interactions and the double derivatives make up the elements of the force constant matrix

$$\mathbf{\Phi}_{l,\kappa,i;l',\kappa',j} = \frac{\partial V}{\partial u_{l,\kappa,i} \partial u_{l',\kappa',j}} \tag{38}$$

where $\Phi_{l,\kappa,i;l',\kappa',j}$ is the force exerted in the i direction on atom κ in unit cell l, when atom atom κ' in unit cell l' is displaced a unit distance in the j direction. The elements of the force constant matrix can be determined either by making small displacements of the atoms in one unit cell, with all other atoms held fixed, and determining the forces on all other atoms—the finite displacement method (Kresse et al. 1995; Alfé 2009), or from perturbation theory (Gonze and Lee 1997; Baroni et al. 2001).

The equations of motion of the system can be expressed

$$m_\kappa \frac{\partial^2 u_{l,\kappa,i}}{\partial t^2} = -\sum_{l',\kappa',j} \phi_{l,\kappa,i;l',\kappa',j} u_{l',\kappa',j} \tag{39}$$

where m_κ is the mass of atom κ. If we assume a harmonic solution to Equation (38) we have

$$u_{l,\kappa,i} = \frac{1}{\sqrt{m_\kappa}} u_{\kappa,i} \exp[-i(\omega t + \mathbf{q} \bullet \mathbf{x}_l)] \tag{40}$$

where ω is the mode frequency, t time, $\mathbf{q}$ mode wave vector and $\mathbf{x}_l$ the coordinates of unit cell l. Substituting this into Equation (39) we obtain

$$\omega^2(\mathbf{q})u_{\kappa,i} = \sum_{\kappa',j} D_{\kappa,i;\kappa',j}(\mathbf{q})u_{\kappa',j} \tag{41}$$

where the dynamical matrix, $D_{\kappa,i;\kappa',j}(\mathbf{q})$, is

$$D_{\kappa,i;\kappa',j}(\mathbf{q}) = \frac{1}{\sqrt{m_\kappa m_{\kappa'}}} \sum_{l'} \Phi_{0,\kappa,i;l',\kappa',j} \exp[-i\mathbf{q}\bullet\mathbf{x}_{l'}] \tag{42}$$

Diagonalization of the dynamical matrix yields the phonon eigenmodes and their frequencies, which allows the determination of both $c_{\mathbf{q},s}$ and $v_{\mathbf{q},s}$ in Equation (7), but in order to calculate lattice thermal conductivity $\tau_{\mathbf{q},s}$ is also needed. In the harmonic approximation the phonon lifetime is infinite and is only limited by anharmonicity, i.e., phonon-phonon interactions, which must be computed using a method other than quasi-harmonic lattice dynamics. In principle anharmonicity will also cause shifts of the mode frequencies, although this effect is typically small for computations of the thermal conductivity (Fig. 5). Estimates of $\tau_{\mathbf{q},s}$ can be obtained from molecular dynamics simulations (de Koker 2009; Turney et al. 2009). One method is to use the Fourier transform of the velocity autocorrelation function to determine the vibrational spectrum at individual wave vectors (Fig. 5) and relate relaxation times to the width of spectral peaks (de Koker 2009). Other techniques include fitting the phonon potential energy autocorrelation function (Turney et al. 2009). Thus by performing both lattice dynamics and molecular dynamics of the same system it is possible to determine its lattice thermal conductivity.

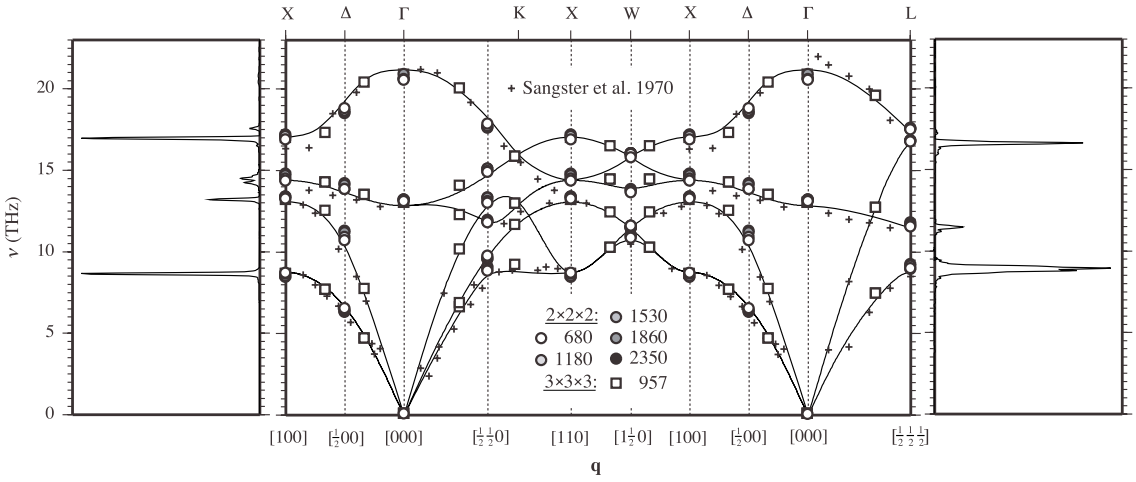

Figure 5. (*center*) Phonon frequencies of MgO periclase calculated from first-principles molecular dynamics (circles; temperature in Kelvin) and first-principles lattice dynamics in the quasi-harmonic approximation (lines). The black crosses are experimental values Sangster et al. (1970). (*left and right panels*) Examples of spectral peaks calculated from first-principles molecular dynamics, at [100] and [½ ½ ½], used to determine phonon relaxation times. Reprinted with permission from de Koker (2009) Physical Review Letters, Vol. 103, Article #125902. Copyright 2009 by the American Physical Society. *http://link.aps.org/doi/10.1103/PhysRevLett.103.125902*

Anharmonic lattice dynamics method

It is also possible to estimate lattice thermal conductivity from lattice dynamics calculations alone, by considering higher order terms in the Taylor expansion (Eqn. 37) (e.g., Broido et al. 2007; Tang and Dong 2009; Turney et al. 2009). In doing so it is possible to determine

relaxation times and anharmonic frequencies. Aside from the pertubative treatment of the anharmonic terms, the Taylor series is also typically truncated, neglecting part of the anharmonic contributions, which can lead to approximations in computed thermal conductivity values.

DISCUSSION

Having described the various approaches for calculating lattice thermal conductivity, we now discuss the relative advantages and disadvantages of each, in an attempt to provide some general guidance on selecting the most appropriate method. Of course, as is the case in all theoretical investigations, this will involve making a compromise between speed and precision, and consideration of available computational resources. Since there have been only a handful of investigations that have used the transient non-equilibrium molecular dynamics method and lattice dynamics techniques, we focus on the Green-Kubo and non-equilibrium molecular dynamics methods, which make up the majority of studies in the literature.

If one considers the Green-Kubo method, a clear advantage is that the entire lattice thermal conductivity tensor can be calculated from one simulation. This is in contrast to the non-equilibrium molecular dynamics methods, which necessitates several simulations in each direction, to achieve the same. This could be an important consideration, if the mineral of interest is known to be anisotropic. The Green-Kubo method also requires less experimentation than non-equilibrium molecular dynamics methods, there being no need to investigate the effect of section size or heat flux on results. On the other hand, it can take a long time for the correlation function to decay to zero, thus long simulations are often required. In addition, the Green-Kubo method requires the identification of the self-energy of each atom, which is not straightforward in the context of first-principles calculations, meaning that it is, for the most part, limited to the study of those phases which are well described by a set of empirical pair potentials.

This issue of empirical pair potentials versus first-principles computation of forces is an important one. Due to the large size and length of simulations that must performed in calculations of lattice thermal conductivity, nearly all previous theoretical investigations have utilized empirical pair potentials to describe the forces between atoms. Using such pair potentials large simulation cells can be used, containing thousands of atoms, and it is possible to model polycrystalline systems and the influence of grain boundaries (e.g., Shukla et al. 2008). However, pair potentials are, in general, parameterized using experimental data determined at ambient conditions or values from static first-principles calculations. It is thus uncertain how well they are able to describe the motion of atoms at lower mantle temperature and pressures. On the other hand, forces determined from first-principles, via the Hellmann-Feynman theorem (Hellmann 1937; Feynman 1939) are parameter free and therefore expected to be more reliable.

Non-equilibrium molecular dynamics simulations can be performed using both empirical pair potentials or within the framework of first-principles calculations. Calculating forces from first-principles increases the computational resources required, which means that much smaller simulation cells must be used, leading to increased finite size effects. However, it has been shown that these can be dealt with in a systematic manner, although it should be noted that because of the nature of the reciprocal plot, associated error-bars can be large for systems with high lattice thermal conductivities (Stackhouse et al. 2008). Of the non-equilibrium molecular dynamics methods, the imposed heat-flux method requires smaller simulation cells, as compared to the transient method. This is because the size of the simulation cell limits the number of sections and many more sections are required to define a sinusoidal temperature perturbation than a linear temperature gradient.

It should also be pointed out that all of the molecular dynamics based methods discussed describe the motion of the atoms using classical mechanics, i.e., by solving Newton's equations of motions. This is true even for *ab initio* molecular dynamics simulations, where, although

the forces are determined from first-principles, atomic motion is still described by classical mechanics, which generates errors at very low temperatures due to quantum effects on the dynamics (Jund and Jullien 1999). However, this is not expected to be a concern when calculating values for minerals at lower mantle temperatures, far above their estimated Debye temperatures.

Quantum effects are included in lattice dynamics calculations. In addition, like the Green-Kubo method, lattice dynamics should also be able to determine the full lattice thermal conductivity tensor. In general, lattice dynamics studies use forces calculated from first-principles, in order to obtain accurate mode frequencies and lifetimes, but the computational resources required to perform a combined lattice and molecular dynamics investigation is still likely to be less than that required for non-equilibrium molecular dynamics studies, at least for simple structures. In more complex structures, such as silicate perovskite, the task of computing the vibrational spectrum and identifying each mode may prove formidable.

In view of all the above, if computational resources allow, we recommend performing first-principles non-equilibrium molecular dynamics simulations to calculate the lattice thermal conductivity of minerals. This avoids concerns regarding the robustness of empirical pair potentials. However, empirical pair potentials may perform well at lower temperatures and pressures, as will be seen in the next section, and in this case they can be used.

THE LATTICE THERMAL CONDUCTIVITY OF PERICLASE

Periclase is the pure magnesium end-member of ferropericlase, thought to be the second most abundant phase in the lower mantle. The simple rock-salt structure of the phase makes it an ideal mineral on which to test new methods. In all, there have been five studies of the lattice thermal conductivity of periclase: one based on the Green-Kubo method (Cohen 1998); two using non-equilibrium molecular dynamics simulations (Shukla et al. 2008; Stackhouse et al. 2008); one using a combination of lattice dynamics and equilibrium molecular dynamics simulations (de Koker 2009) and one using anharmonic lattice dynamics (Tang and Dong 2009). The phase has thus been studied using almost all of the methods described in the previous section. The results of these investigations are compared with available experimental data in Figures 6. Note that, Tang and Dong (2009) only reported temperature and pressure derivatives. The results of Stackhouse et al. (2008) are still under review and are not shown.

If we first consider the ambient pressure data, one can see that the Green-Kubo calculations of Cohen (1998), based on a non-empirical ionic model, predict values a little lower than experimental values and those from other theoretical studies. The results of the non-equilibrium molecular dynamics simulations that used pair potentials (Shukla et al. 2008) agree well with experiment, in particular, those of Hofmeister and Yuen (2007). This suggests that empirical pair potentials can perform well at low pressures. The first-principles non-equilibrium molecular dynamics calculations of Stackhouse et al. (2008), also agree well with experimental values, in particular, those of Kanamori et al. (1968). Moving to high pressure, we find that the first-principles calculations of de Koker (2009) predicts values in good agreement with the experimental data of Goncharov et al. (2009), which fall between the two theoretical predictions (Fig. 6).

It should be noted that the values determined in the theoretical studies discussed are for perfect periclase single crystals, which do not contain iron impurities or defects. In the lower mantle, ferropericlase exists in polycrystalline form and grain boundaries, and defects, such as iron impurities will increase phonon scattering, decreasing the lattice thermal conductivity of the phase. The lattice thermal conductivity of periclase should therefore be viewed as an upper bound to that of ferropericlase. In their non-equilibrium molecular dynamic simulations, Shukla et al. (2008) investigated the effect of grain boundary scattering on the lattice thermal conductivity of periclase, finding it to be significant at low temperatures, while at higher

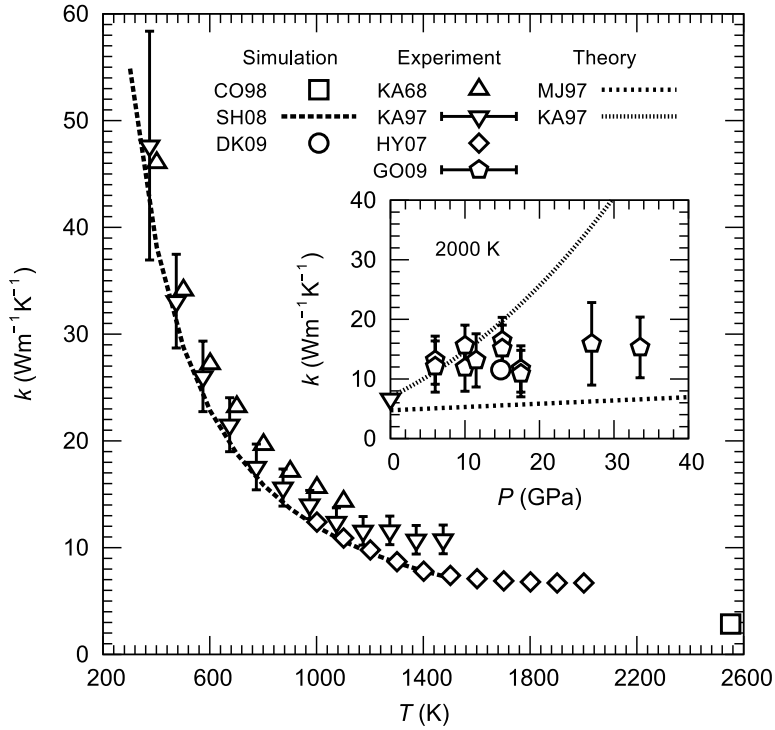

Figure 6. The lattice thermal conductivity of periclase as a function of temperature at 0 GPa (*main*) and as a function of pressure at 2000 K (*inset*). Simulation values: CO90 (Cohen 1998); SH08 (Shukla et al. 2008); DK09 (de Koker 2009). Experimental values: KA68 (Kanamori et al. 1968); KA97 (Katsura 1997); HY07 (Hofmeister and Yuen 2007); GO09 (Goncharov et al. 2009). Theoretical values: MJ97 (Manga and Jeanloz 1997); KA97 (Estimated from results of Katsura 1997). Best agreement with experiment is found for the non-equilibrium molecular dynamics simulations (Shukla et al. 2008).

temperatures, such as those expected in the lower mantle, the effect was small. This is because at high temperatures the phonon mean free path is smaller than the grain size, while at lower temperatures they may be comparable. The influence of grain size will therefore depend on the intrinsic lattice thermal conductivity of the single crystal. The effect of defects, such as iron impurities, remains to be quantified in periclase.

CONCLUSION

Determining the thermal conductivity of lower mantle minerals is important for constraining many important processes in both the past and present deep Earth. In light of the experimental difficulties in measuring thermal conductivity, theoretical methods offer an invaluable alternative. There exist a number of different theoretical techniques, which have been used in the field of materials science, which can also be applied to mantle minerals. Each of these methods have advantages and disadvantages, and the appropriate method must be chosen in a compromise between speed and accuracy. Studies of periclase indicate, at present, that non-equilibrium molecular dynamics simulations are promising and will be readily scaled to more complex crystal structures.

ACKNOWLEDGMENTS

The authors are indebted to Nico de Koker for helpful discussions and an early copy of his manuscript.

REFERENCES

Alfé D (2009) PHON: A program to calculate phonons using the small displacement method. Comput Phys Commun 180:2622-2633

Allen MP, Tildesley DJ (1987) Computer Simulation of Liquids. Clarendon Press, Oxford, United Kingdom

Badro J, Fiquet G, Guyot F, Rueff J-P, Struzhkin VV, Vankó G, Monaco G (2003) Iron partitioning in earth's mantle: towards a deep lower mantle discontinuity. Science 305:383-386

Badro J, Rueff J-P, Vankó G, Monaco G, Fiquet G, Guyot F (2004) electronic transitions in perovskite: possible nonconvecting layers in the lower mantle. Science 300:789-791

Baroni S, de Gironcoli S, Dal Corso A, Giannozzi P (2001) Phonons and related crystal properties from density-functional perturbation theory. Rev Mod Phys 73:515-562

Broido, DA, Malory M, Birner G., Mingo N, Stewart DA (2007) Intrinsic lattice thermal conductivity of semiconductors from first principles. Appl Phys Lett 91:231922

Chantrenne P (2007) Molecular dynamics. Top Appl Phys 107:155-180

Chantrenne P, Barrat J-L (2004) finite size effects in determination of thermal conductivities: comparing molecular dynamics results with simple models. J Heat Trans 126:577-585

Cohen RE (1998) Thermal conductivity of MgO at high pressures. Rev High Pres Sci Tech 7:160-162

Daly BC, Maris HJ (2002) Calculation of the thermal conductivity of superlattice by molecular dynamics simulation. Physica B 316:247-249

Daly BC, Maris HJ, Imamura K, Tamura S (2002) Molecular dynamics calculation of the thermal conductivity of superlattices. Phys Rev B 66:024301

de Koker N (2009) Thermal conductivity of MgO periclase from equilibrium first principles molecular dynamics. Phys Rev Lett 103:125902

Dubuffett F, Yuen DA (2000) A thick pipe-like heat-transfer mechanism in the mantle: nonlinear coupling between 3-D convection and variable thermal conductivity. Geophys Res Lett 27:17-20

Dubuffet F, Yuen DA, Rabinowicz M (1999) Effects of a realistic mantle thermal conductivity on the patterns of 3-D convection. Earth Planet Sci Lett 171:401-409

Evans DJ, Morris GP (1990) Statistical Mechanics of Non-Equilibrium Liquids. Academic Press, London, United Kingdom

Feynman RP (1939) Forces in molecules. Phys Rev 56:340-343

Goncharov AF, Struzhkin VV, Jacobsen SD (2006) reduced radiative conductivity of low-spin (Mg,Fe)O in the lower mantle. Science 312:1205-1208

Goncharov AF, Haugen BD, Struzhkin VV, Beck P, Jacobson SD (2008) Radiative conductivity in the Earth's lower mantle. Nature 456:231-234

Goncharov AF, Beck P, Struzhkin VV, Haugen BD, Jacobsen SD (2009) Thermal conductivity of lower-mantle minerals. Phys Earth Planet Inter 174:24-32

Gonze X, Lee C (1997) Dynamical matrices, born effective charges, dielectric permittivity tensors, and interatomic force constants from density-functional perturbation theory. Phys Rev B 55:10355-10368

Green MS (1954) Markoff random processes and the statistical mechanics of time-dependent phenomena. II Irreversible processes in fluids. J Chem Phys 22:398-413

Gubbins D, Willis AP, Sreenivasan B (2007) Correlation of Earth's magnetic field with lower mantle thermal and seismic structure. Phys Earth Planet Inter 162:256-260

Hellmann H (1937) Einführung in die Quantenchemie. Franz Deuticke, Leipzig, Deutchland

Hofmeister AM (2007) Pressure dependence of thermal transport properties. Proc Nat Acad Sci USA 104:9192-9197

Hofmeister AM (2008) Inference of high thermal transport in the lower mantle from laser-flash experiments and the damped harmonic oscillator model. Phys Earth Planet Inter 170:201-206

Hofmeister AM, Yuen DA (2007) Critical phenomena in thermal conductivity: Implications for lower mantle dynamics. J Geodyn 44:186-199

Holman JP (1976) Heat Transfer. McGraw-Hill, New York, United State of America.

Jund P, Jullien R (1999) Molecular-dynamics calculation of the thermal conductivity of vitreous silica. Phys Rev B 59:13707-13711

Kanamori H, Fujii N, Mizutani H (1968) Thermal diffusivity measurement of rock-forming minerals from 300 degrees to 1100 degrees K. J Geophys Res 73:595-605

Katsura T (1997) Thermal diffusivity of periclase at high temperature and high pressures. Phys Earth Planet Inter 101:73-77

Keppler H, Kantor I, Dubrovinsky LS (2007) Optical absorption spectra of ferropericlase to 84 GPa. Am Mineral 92:433-436

Keppler H, Dubrovinsky LS, Narygina O, Kantor I (2008) Optical absorption and radiative thermal conductivity of silicate perovskite to 125 gigapascals. Science 322:1529-1532

Kreith F, Bohn MS (2001) Principles of Heat Transfer. Brooks-Cole, Pacific Grove, California, United States of America

Kresse G, Furthmuller J, Hafner J (1995) Ab initio force constant approach to phonon dispersion relations of diamond and graphite. Europhys Lett 32:729-734

Kubo R (1957), Statistical mechanical theory of irreversible processes. I. General theory and simple applications to magnetic and conduction problems. J Phys Soc Japan 12:570-586

Kubo R (1966) The fluctuation-dissipation theorem. Rep Prog Phys 29:255-284

Ladd AJC, Moran B., Hoover WG (1986) Lattice thermal conductivity: A comparison of molecular dynamics and anharmonic lattice dynamics. Phys Rev B 34:5058-5064

Lay T, Hernlund J, Buffett BA (2008) Core-mantle boundary heat flow. Nat Geosci 1:25-32

Leach AR (2001) Molecular Modelling: Principles and Applications. Pearson Education Limited, Harlow, United Kingdom

Lee KKM, O'Neill B, Panero WR, Shim SH, Benedetti LR, Jeanloz R (2004) Equations of state of the high-pressure phases of a natural peridotite and implications for the Earth's lower mantle. Earth Planet Sci Lett 223:381-393

Mahajan SS, Subbarayan G, Sammakia BG (2007) Estimating thermal conductivity of amorphous silica nanoparticles and nanowires using molecular dynamics simulations. Phys Rev E 76:056701

Manga M, Jeanloz R (1997) Thermal conductivity of corundum and periclase and implications for the lower mantle. J Geophys Res 102:2999-3008

Maradudin AA, Montroll EW, Weiss GH (1963) Theory of Lattice Dynamics in the Harmonic Approximation. Academic Press, New York and London, United Kingdom

McGaughey AJH, Kaviany M (2006) Phonon transport in molecular dynamics simulations: formulation and thermal conductivity prediction. Adv Heat Trans 39:169-225

Mountain RD (2006) System size and control parameter effects in reverse perturbation nonequilibrium molecular dynamics. J Chem Phys 124:104109

Müller-Plathe F (1997) A simple nonequilibrium molecular dynamics method for calculating the thermal conductivity. J Chem Phys 106:6082-6085

Naliboff JB, Kellogg LH (2006) Dynamic effect of a step-wise increase in thermal conductivity and viscosity in the lowermost mantle. Geophys Res Lett 33:L12S09

Naliboff JB, Kellogg LH (2007) Can large increases in viscosity and thermal conductivity preserve large-scale heterogeneity in the mantle. Phys Earth Planet Inter 161:86-102

Nieto-Draghi C, Avalos JB (2003) Non-equilibrium momentum exchange algorithm for molecular dynamics simulation of heat flow in multicomponent systems. Mol Phys 101:2303-2307

Nye JF (1987) Physical Properties of Crystals: Their Representation by Tensors and Matrices. Oxford University Press, Oxford, United Kingdom

Sangster MJ, Peckham G, Saunderson DH (1970) Lattice dynamics of magnesium oxide. J Phys C 3:1026-1036

Schelling PK, Phillpot SR, Keblinski P (2002) Comparison of atomic-level simulation methods for computing thermal conductivity. Phys Rev B 65:144306

Shukla P, Watanabe T, Nino JC, Tulenko JS, Phillpot SR (2008) Thermal transport properties of MgO and Nd_2ZrO_7 pyrochlore by molecular dynamics simulation. J Nucl Mater 380:1-7

Srivastava GP (1990) The Physics of Phonons. Taylor & Francis Group, New York, United States of America

Stackhouse S, Stixrude L, Karki BB (2008) The thermal conductivity of periclase (MgO) from first-principles. EOS Trans AGU 89, Fall Meeting Supp. Abs. # MR21C

Sun L, Murthy J (2006), Domain size effects in molecular dynamics simulation of phonon transport in silicon. Appl Phys Lett 89:171919

Tang XL, Dong JJ (2009) Pressure dependence of harmonic and anharmonic lattice dynamics in MgO: A first-principles calculation and implications for lattice thermal conductivity. Phys Earth Planet Inter 174:33-38

Turney JE, Landry ES, McGaughey AJH, Amon CJ (2009) Predicting phonon properties and thermal conductivity from anharmonic lattice dynamics calculations and molecular dynamics simulations. Phys Rev B 79:064301

Volz SG, Chen G (2000) Molecular-dynamics simulation of thermal conductivity of silicon crystals. Phys Rev B 61:2651-2656

Willis AP, Sreenivasan B, Gubbins D (2007) Thermal core-mantle interaction: Exploring regimes for 'locked' dynamo action. Phys Earth Planet Inter 165:83-92

Yoon YG, Car R, Srolovitz DJ, Scandolo S (2004) Thermal conductivity of crystalline quartz from classical simulations. Phys Rev B 70:012302

Ziman JM (1960) Electrons and Phonons. Oxford University Press, Oxford, United Kingdom